Section 7

Global and regional climate models, sensitivity and impact experiments, response to external forcing, monthly and seasonal forecasting.

Estimation of methane emissions from wetlands of Western Siberia and their uncertainty due to climatic noise

S.N. Denisov, M.M. Arzhanov, M.G. Akperov, N.V. Pankratova
A.M. Obukhov Institute of Atmospheric Physics, RAS
denisov@ifaran.ru

The ensemble of numerical experiments with a joint model of the methane cycle and heat and moisture transport in soil was performed forced by data from the atmospheric general circulation model ECHAM5.

Wetland methane emission model consists of two modules. In the methane emission module, the flux of methane from the soil to the atmosphere is calculated using the parameterization of the temperature dependence of methane production by bacteria. It also takes into account the dependence of emissions on the amount of the carbon substrate in the active soil layer [1, 2]. Necessary physical characteristics of the soil are calculated in the module of heat and moisture transport, which can reproduce the dynamics of the soil temperature fields in case of alternating several boundaries of thawed and frozen layers and diagnose the formation of intermediate non-freezing zones (taliks) for several years [3].

An ensemble of 45 realizations of the multi-year data of meteorological variables at the land surface, calculated by the ECHAM5 for different initial and identical boundary conditions for a 34-year period (from 1.01.1979 to 31.12.2012) was specified as space-distributed input data. The initial conditions (the state of the atmosphere for January 1, 1979) were specified as instantaneous atmospheric conditions at various 12 hour intervals in December 1978. Mean values and standard deviations of annual and monthly emission indices were estimated. The 95% confidence intervals were calculated as indices of the variability (due to the internal variability of the climate system) of the mean value estimates and the standard deviation. These indices were calculated under assumption of corresponding estimates to obey the Gaussian probability distribution. The uncertainty of the estimates (mean value and standard deviation) was considered to be the ratio of half the width of the 95% confidence interval of the corresponding estimate to its average value.

Estimations of methane emissions from wetlands in Western Siberia for 1979-2012 periods were obtained (Fig. 1). The ensemble average of annual emissions over the estimated period equals 3.8 TgCH4 (uncertainty index is 10%). Highest methane flux estimations (more than 2 TgCH4) obtained for August-September (Fig. 2). The trend of emissions equals about 0.02 TgCH4/yr. Total annual emissions in individual years may differ by more than 3 times between different realizations of the model. For individual months, the uncertainty index of emission mean values equals 7-35%, and it is minimal for months with maximal emissions. It is concluded that the uncertainty of methane emission mean values due to climatic noise decreases with the growth of the averaging time interval. The uncertainty of the estimates for the emission mean values on the monthly scale has a pronounced seasonal variability. The uncertainty index of the standard deviation estimates for both annual and monthly emission values is 25-26% and has negligible seasonal variability.

This work is supported by Russian Foundation for Basic Research (15-05-02457, 16-07-01205, and 17-05-01097) and RAS.

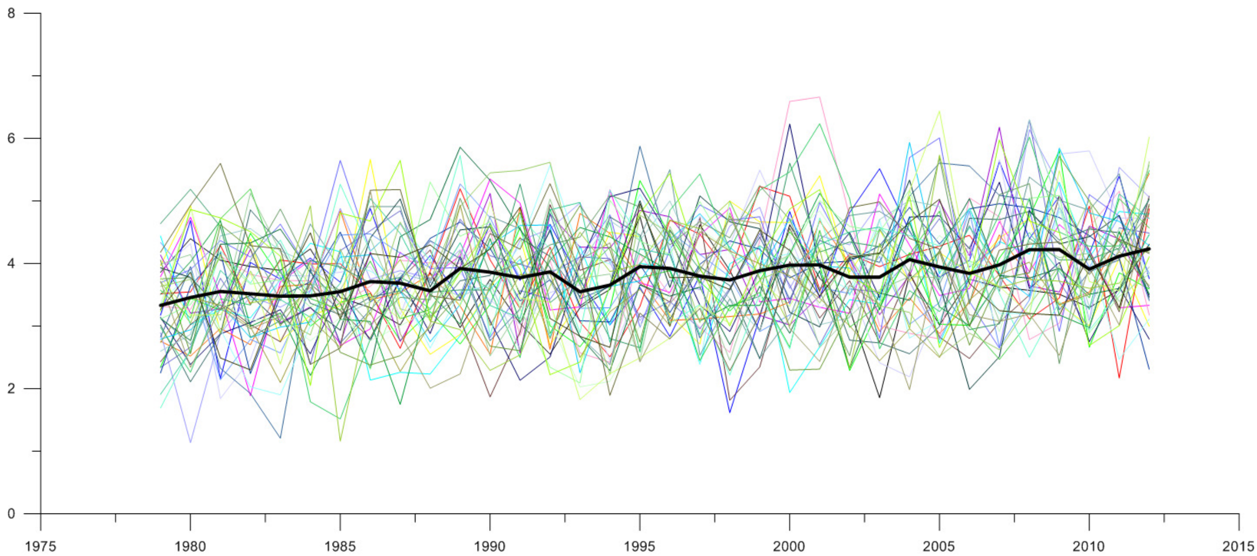

Fig.1 Methane emissions [TgCH4/yr] from Western Siberian wetlands (thick line is the ensemble mean)

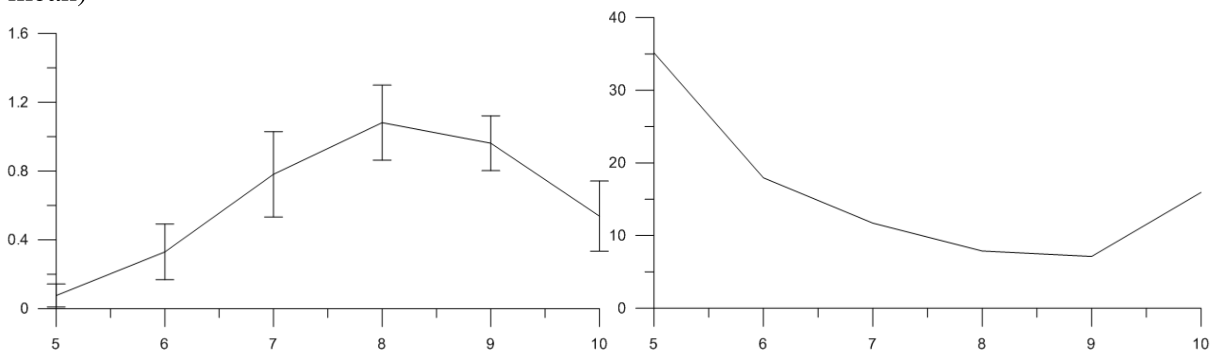

Fig.2 Modeled mean methane emissions [TgCH4/yr] and uncertainty index [%] on monthly scale (month numbers on y axis)

References

[1] Eliseev A.V., Mokhov I.I., Arzhanov M.M., Demchenko P.F., Denisov S. N. Interaction of the methane cycle and processes in wetland ecosystems in a climate model of intermediate complexity // Izv. Atmos. Ocean. Phys. (2008) 44: 139.

[2] Denisov S. N., Eliseev A. V., Mokhov I. I., Arzhanov M.M. Model estimates of global and regional atmospheric methane emissions of wetland ecosystems // Izvestiya Atmospheric and Oceanic Physics V. 51. I. 5. P. 482-487. 2015.

[3] Arzhanov M.M., Eliseev A.V., Mokhov I.I. Impact of climate changes over the extratropical land on permafrost dynamics under RCP scenarios in the 21st century as simulated by the IAP RAS climate model // Russ. Meteorol. Hydrol. (2013) 38: 456.

A new seasonal forecast system for Météo-France: features and performances

Michel Déqué, Constantin Ardilouze, Lauriane Batté, Laurent Dorel, Jean-François Guérémy and Danila Volpi
Centre National de Recherches Météorologiques (CNRS/CNRM), Météo-France.
42 avenue Coriolis F-31057 Toulouse Cédex 1, France, michel.deque@meteo.fr

Since 2004 Météo-France has been part of the Eurosip consortium which builds up each month a 7-month numerical forecast based on several contributors (presently ECMWF, Met Office, NCEP, JMA and Météo-France). Each contribution provides hindcasts of at least 20 years for the 12 starting months. Each contributor updates from time to time his method to produce hindcasts/forecasts named "system". The numerical cost of a full hindcast, together with the time necessary to evaluate a new system, and the need of users for some stability, prevent frequent system upgrades. Météo-France system 5, developed in 2014 and early 2015, was introduced in Eurosip in June 2016. Since early 2016 a new system 6 has been developed. It has been launched in a parallel suite in March 2017 and should replace system 5 in 2018.

Météo-France system 6 upgrade corresponds to the migration from the CMIP5 version of the Météo-France climate model to the CMIP6 version. The so-called atmosphere diagnostic physics described in Voldoire et al. (2013) has been replaced by a prognostic physics in which the diabatic terms take into account the present as well as the past state of the atmosphere (Cuxart et al., 2000 for turbulence; Lopez, 2002 for micro-physics; Guérémy, 2011 for convection). The model components are.

- atmosphere: Arpege 6.0, T255, L91, Δt=15 min (system 5); Arpege 6.2, T359, L91, Δt=7.5 min (system 6)
- ocean: Nemo 3.2, 1°, L42 , Δt=1h (system 5); Nemo 3.6, 1°, L75 Δt=30 min (system 6)
- land surfaces: Surfex 7.3 (system 5); Surfex 8.1 (system 6)
- sea-ice: Gelato 5 (system 5); Gelato 6 (system 6)

For the sake of fair comparison, an additional hindcast experiment has been carried out with the two systems. It is based on 30 members starting on 1st February, 1st May, 1st August and 1st November and lasts 7 months. This hindcast spans the 1993-2015 period. Both ensembles are generated using the stochastic dynamics technique (Batté and Déqué, 2016)

Table 1 shows the root mean square (RMS) systematic error of seasonal average (months 2-4) for 500 hPa height (Z500) in the 30°N-90°N band, and for sea surface temperature (SST)in the 30°S-30°N band. This score, calculated against ERA-interim, measures the accuracy of the simulated climate in the first months of a coupled simulation starting from an observed state. The results show a systematic improvement of system 6 climate versus system 5 one.

	MAM		JJA		SON		DJF	
	Syst. 5	Syst. 6	Syst. 5	Syst. 6	Syst. 5	Syst. 6	Syst. 5	Syst. 6
Z500	34	10	20	15	37	19	45	18
SST	1.0	0.5	0.9	0.6	1.1	0.8	1.0	0.9

Table 1: RMS seasonal bias for 30°N-90°N Z500 (m) and for 30°S-30°N SST (K)

Table 2 shows, for the same variables as Table 1, the mean anomaly correlation coefficient (ACC). This score measures the predictive skill. System 6 is better than or equivalent to system 5, except for autumn northern latitudes circulation.

In winter (DJF), mid-latitude predictability can also be measured by the time correlation of circulation indices. These indices are derived by projecting model anomalies on the first mode of Principal Component Analyses performed with ERA interim data (1979-2012). The time correlations for system 5 / system 6 are:

- Arctic Oscillation (based on northern hemisphere mean sea level pressure): 0.69 / 0.66

- North Atlantic Oscillation (based on North Atlantic/Europe Z500): 0.52 / 0.61
- Pacific North America (based on North Pacific/North America Z500): 0.47 / 0.55

	MAM		JJA		SON		DJF	
	Syst. 5	Syst. 6	Syst. 5	Syst. 6	Syst. 5	Syst. 6	Syst. 5	Syst. 6
Z500	.27	.32	.10	.17	.26	.15	.34	.42
SST	.65	.65	.65	.68	.76	.77	.71	.74

Table 2: Seasonal ACC for 30°N-90°N Z500 and for 30°S-30°N SST

Tropical SST seasonal predictability is maximum in the Pacific Ocean. The skill is often measured by the time coefficient correlation of the SST average in the Nino 3.4 box (5°S-5°N by 170°W-120°W). Figure 1 displays the time correlation with respect to ERA-interim SST of the monthly means as a function of the lead time and shows the improvement brought by system 6, except in spring (MAM).

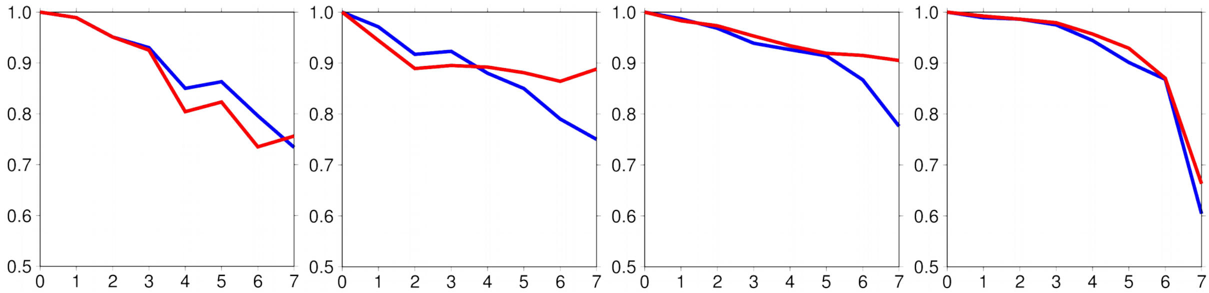

1st February start   1st May start   1st August start   1st November start

Figure 1: Nino 3.4 monthly SST correlation as a function of the lead time (month); system 5 (blue line) and system 5 (red line)

In conclusion, this new system has a more realistic climate and is in many aspects better than the previous one in terms of predictability. It will be implemented in the future European multi-model seasonal prediction developed in the framework of the Copernicus Climate Change Services (C3S).

This work has been supported by the C3S-433 contract of the Copernicus European Union program.

References:

Batté, L. and Déqué, M., 2016: Randomly correcting model errors in the ARPEGE-Climate v6.1 component of CNRM-CM: applications for seasonal forecasts. Geosci. Model Dev. 9:2055-2016, DOI:10.5194/gmd-9-2055-2016

Cuxart, J., Bougeault, Ph. and Redelsperger, J-L., 2000 : A turbulence scheme allowing for mesoscale and large-eddy simulations. Quart. J. R. Met. Soc., 126, 1-30.

Guérémy, J. F., 2011 : A continuous buoyancy based convection scheme: one and three dimensional validation. Tellus A, 63, 687-706.

Lopez, Ph., 2002 : Implementation and validation of a new prognostic large-scale cloud and precipitation scheme for climate and data-assimilation purposes. Quart. J. R. Met. Soc., 128, 229-257.

Voldoire, A.**,** E. Sanchez-Gomez, D. Salas y Mélia, B. Decharme, C. Cassou, S.Sénési, S. Valcke, I. Beau, A. Alias, M. Chevallier, M. Déqué, J. Deshayes, H. Douville, E. Fernandez, G. Madec, E. Maisonnave , M.-P. Moine, S. Planton, D. Saint-Martin, S. Szopa, S. Tyteca, R. Alkama, S. Belamari, A. Braun, L. Coquart and F. Chauvin., 2013: The CNRM-CM5.1 global climate model : description and basic evaluation , Clim. Dyn., DOI:10.1007/s00382-011-1259-y

Improved Representation of Clouds in Climate Model MRI-ESM2

Hideaki Kawai[1] (h-kawai@mri-jma.go.jp), Seiji Yukimoto[1], Tsuyoshi Koshiro[1], Naga Oshima[1], Taichu Tanaka[1], and Hiromasa Yoshimura[1]

[1]*Meteorological Research Institute, JMA*

1. Introduction

The previous version of the climate model of MRI MRI-CGCM3 (Yukimoto et al. 2012; TL159L48 in the standard configuration), which was used for CMIP5 simulations, had various limitations in terms of representation of clouds. In the updated version of our climate model, MRI-ESM2 (TL159L80), which is planned for use in CMIP6 simulations, the representations of clouds and aerosol–cloud interactions are improved. Figure 1 shows that the biases in shortwave cloud radiative effect are substantially reduced in the new version. The main improvements are briefly summarized herein.

2. Improvements and Results

(i) New Stratocumulus Parameterization

New stratocumulus parameterization based on a stability index that considers a cloud-top entrainment criterion (Kawai 2013; Kawai et al. 2017) was introduced. Vertical mixing at the top of a boundary layer is suppressed when the stability is high, promoting stratocumulus occurrence. There was a significant shortwave radiative flux bias (underestimated reflection of solar insolation) over the Southern Ocean in the old version, as observed in the case of many climate models. However, the bias was considerably reduced mainly due to the increased low-level cloud cover by the introduction of new stratocumulus parameterization (figure is not shown; see Kawai 2013).

(ii) Supercooled Water

In the old model, excessive ice-phase clouds and rare supercooled liquid clouds were observed over the Southern Ocean, as compared with CALIPSO satellite observation data. In the new version, the treatment of the Wegener–Bergeron–Findeisen process was modified, taking into account a relationship between liquid:ice ratio and temperature derived by Hu et al. (2010). This modification resulted in an increase in the ratio of supercooled liquid clouds in the new version, and this result is consistent with the satellite data (Fig. 2). The change in the phase ratio also contributed to the increase in the reflection of solar insolation and reduction in shortwave radiation bias over the area. This is because the effective radius of a cloud droplet is much smaller than that of ice crystals and the optical thickness of the clouds increased because of the change.

(iii) Vertical Resolution

The vertical resolution was increased from L48 to L80, and the number of vertical layers in an atmospheric boundary layer was nearly doubled in MRI-ESM2 (from 5 to 10 layers below 900 hPa). This increase helped in resolving the problem of excessive geometric thickness of low-level clouds that have extremely high albedo (Fig. 3).

(iv) Stratocumulus to Cumulus Transition

In the old model, the vertical structures of low-level clouds transition from stratocumulus to cumulus off Peru were unrealistic. However, they were significantly improved in the new version (Fig. 4) by preventing the occurrence of shallow convection over the area where the conditions for stratocumulus occurrence [see Item (i)] are met.

(v) Cloud Overlap

In the old version, the treatment of cloud overlap in the shortwave radiation calculation caused excessive reflection of solar radiation, particularly for deep convection towers topped by anvil clouds. In the new version, a more realistic cloud overlap became available in the shortwave radiation calculation because of the introduction of practical independent column approximation (PICA; Nagasawa 2012). This new cloud overlap scheme enabled the drastic alleviation of excess reflection of shortwave radiation over the tropics (figure is not shown).

(vi) Horizontal Resolution for Radiation

Though the horizontal resolution is TL159 for both models, in the old version, full radiation computations were

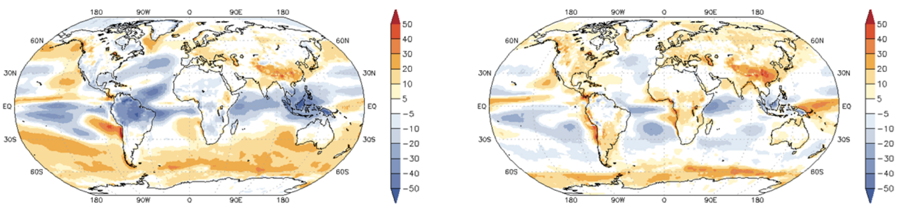

Fig. 1: Biases in shortwave cloud radiative effect (W/m^2) based on historical CMIP simulations using MRI-CGCM3 (left) and MRI-ESM2 (right). Annual means for the period 1986–2005. Observation is CERES-EBAF.

performed for every two grids in the zonal direction. In the new version, these calculations are performed for each model grid. The low-level clouds in the subtropics and mid-latitudes slightly increased because of this change (Fig. 5), presumably due to the improvement in the cloud–radiation interactions.

(vii) Bug Fixes

The old version had a bug associated with the prognostic equations of number concentrations of the cloud particles. This bug caused the problem of large number concentrations of cloud particles, particularly, for stratocumulus and stratus over the subtropics and northern Pacific region. In addition, the bug caused a large decrease in the number concentration of cloud droplets and large positive cloud feedback for such clouds in warmer climate simulations. This bug was fixed in the new version.

(viii) Aerosol Mode Radii

Aerosol mode radii were modified based on recent observations. Consequently, appropriate number concentrations of cloud particles were achieved. In particular, the increase in the mode radii of organic carbon from 0.0212 to 0.1 μm caused a significant decrease in the cloud droplet number concentration that originated from organic carbon. This modification significantly decreased the aerosol–cloud interactions associated with organic carbon.

(ix) Cloud Ice Fall

The calculation method of cloud ice fall in the old version was inappropriate, and it caused unrealistic calculation of ice fall and large time-step dependency of ice water content. The main problem was that the ratio of snow, which is removed from the ice water content at each time step and falls down to the surface within one time step, was not proportional to the time step. The treatment of cloud ice fall was improved based on the study of Kawai (2005), and the time-step dependency was alleviated (figure is not shown).

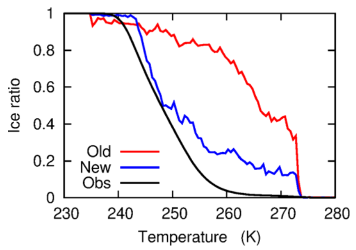

Fig. 2: Ice ratio in MRI-CGCM3 (old version; red line), MRI-ESM2 (new version; blue), and Hu et al. (2010) (observation; black). Global mean at 700 hPa for January.

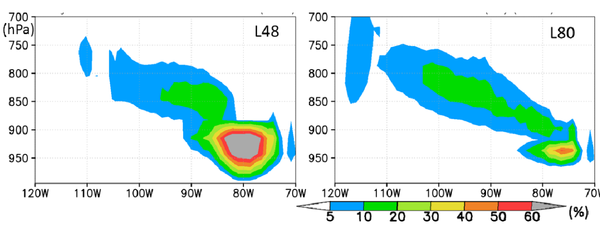

Fig. 3: Cross sections of cloud fraction along 20°S using models with vertical resolution L48 (left) and L80 (right) for January.

Acknowledgements

These improvements were achieved owing to the valuable information obtained from multiple model intercomparison studies and projects. This work was supported in part by the "Program for Risk Information on Climate Change (SOUSEI)" and TOUGOU of the Ministry of Education, Culture, Sports, Science and Technology (MEXT), Japan. Additionally, it was supported by the Japan Society for the Promotion of Science (JSPS) and the Global Environment Research Fund (2-1403 and 2-1703) of the Ministry of the Environment, Japan.

References

Hu, Y., et al., 2010: Occurrence, liquid water content, and fraction of supercooled water clouds from combined CALIOP/IIR/MODIS measurements. *J. Geophys. Res. Atmos.*, **115**, 1–13.

Kawai, H., 2005: Improvement of a cloud ice fall scheme in GCM. *WGNE Blue Book*, **35**, 4.11–4.12.

Kawai, H., 2013: Improvement of a stratocumulus scheme for mid-latitude marine low clouds. *WGNE Blue Book*, **43**, 4.03–4.04.

Kawai, H., et al., 2017: Indexes and parameters related to low cloud cover and low cloud feedback. *J. Climate*, under review.

Nagasawa, R., 2012: The problem of cloud overlap in the radiation process of JMA's Global NWP Model. *WGNE Blue Book*, **42**, 04.15–04.16.

Yukimoto, S., et al., 2012: A new global climate model of Meteorological Research Institute: MRI-CGCM3 -- model description and basic performance --. *J. Meteor. Soc. Japan*, **90A**, 23–64.

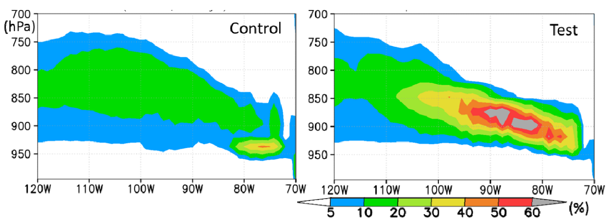

Fig. 4: Same as Fig. 3; however, this figure shows a comparison between using original shallow convection calculation (left) and a treatment of shallow convection suppressed under stratocumulus condition (right), which is calculated by a model with L80 vertical resolution.

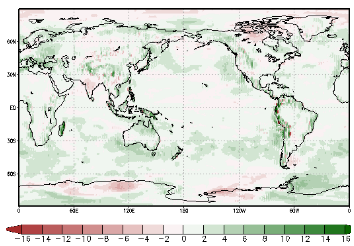

Fig. 5: Impact on the low-level cloud cover (%) by a change in radiation computation from every two grids to every grid in the zonal direction (annual mean).

Multiple climatic regimes in transitional seasons

Mokhov I.I.

A.M. Obukhov Institute of Atmospheric Physics RAS
Lomonosov Moscow State University
mokhov@ifaran.ru

During last decades an increase in climatic variability is detected. In particular, very extreme was spring in Russian regions in 2017 with very warm March and cold air outbreaks in May (and even in June). In the last 5 years (2012-2016), the number of hazardous meteorological events in Russian regions has been almost three times more than for 1998-2002 (http://www.meteorf.ru/). Analysis of intraseasonal variability of surface air temperature from long-term observations reveals multimodal features in probability density functions (PDF), in particular for transitional (spring, autumn) seasons (Agayan and Mokhov, 1989; Mokhov and Semenov, 1997; Mokhov et al., 1998).

In (Mokhov and Semenov, 1997), an analysis of bimodal features of PDF for intra-seasonal variations of surface air temperature using a stochastic energy balance model and daily data from long-term (since the end of the 19th century) observations at many Eurasian meteorological stations was performed. The PDF polymodality can be formed by different processes. In particular, the formation of the PDF bimodality can be related to the nonlinear temperature dependence of surface albedo near the snow boundaries.

Mokhov and Semenov (1997) used the energy balance equation

$$C\partial T/\partial t = F_S - F_T - \text{div } F + w(t)$$

in terms of a zonal surface temperature $T(\varphi)$. Here: $F_S = QS(1-\alpha(T))$, QS - insolation, α – albedo, $F_T = A + BT$ - outgoing long-wave radiation (A, B – constants), *C* - parameter characterizing the heat capacity of the climatic system, div $F = \gamma(T-T_H)$ – meridional heat influx, T_H – hemispheric mean temperature, γ – parameter characterizing the meridional heat transfer, w(t) - Gaussian random source, φ - latitude. In general, the efficiency of meridional heat transfer (and parameter γ) depends on climatic conditions (Vasyuta et al., 1988; Rind and Chandler, 1991).

Albedo α is considered as a function of temperature T, antisymmetric relative to Ts = 0^{o}C - temperature of snow/ice cover boundary

$$\alpha(T) = \alpha_o - (1/2)\Delta\alpha f(T-T_s),$$

where parameter $\Delta\alpha$ characterizes change of albedo at the snow/ice cover boundary.

According to (Mokhov and Semenov, 1997) the PDF for temperature anomalies has three extremes, including two maxima and minimum near Ts, if

$$T^* > T^o,$$

where $T^* = (1/2)QS\Delta\alpha/(B+\gamma)$, $T^o = (df/dT)^{-1}$. In (Mokhov and Semenov, 1997) using analytic parametrization of the albedo, analytical expressions are obtained for the PDF maxima position ΔT relative to Ts = 0^{o}C

$$\Delta T^2 = T^{*2} - T^{o2}.$$

The sensitivity of ΔT to the climate (temperature) change can be estimated from the next expression

$$\Delta T d\Delta T/dT = T^* dT^*/dT - T^o dT^o/dT.$$

In particular, the decrease of $\Delta\alpha$ under warming ($dT > 0$) contributes to a decrease of ΔT. Decrease (or increase) of climate anomalies near 0^oC with snow/ice cover variations depends also on changes of the efficiency of meridional heat transfer.

This work was carried out within the framework of RFBR projects and RAS programs.

References

Agayan G.M. and I.I. Mokhov (1989) Quasistatiomary autumn atmospheric regimes of the Northern Hemisphere during the period of the FGGE. *Izvestiya, Atmos. Oceanic Phys.*, **25**, 851-855.

Mokhov I.I., Semenov V.A., 1997: Bimodality of the probability density functions of subseasonal variations in surface air temperature. *Izvestiya, Atmos. Oceanic Phys.*, **33**, 702-708.

Mokhov I.I., V.K. Petukhov and V.A. Semenov (1998) Multiple intraseasonal temperature regimes modelling of trends of the Earth's climate variability characteristics. *Izvestiya, Atmos. Oceanic Phys.*, **34**, 163-171.

Rind D. and M. Chandler (1991) Increased ocean heat transports and warmer climate. *J. Geophys. Res.*, **96**(D4), 7437-7461.

Vasyuta Yu.B., I.I. Mokhov and V.K. Petukhov (1988) Sensitivity of low-parametric climate models to variations of characteristics of meridional heat flux. *Izvestiya, Atmos. Oceanic Phys.*, **24**, 85-92.

Paleoclimate modeling experiments

Valeriy Parkhomenko

Dorodnicyn Computing Centre, FRC CSC RAS
Moscow, Russia; parhom@ccas.ru

Selecting the periods of the Earth evolution for climate modeling numerical experiments, we decided to choose those with the greatest differences in the continent pattern. Only the relatively late stages of evolution were considered so that more or less accurate data of the solar constant, the CO_2 concentration and continents configuration could be used [1].

Climate modelling was carried out for two periods of the Earth evolution characterized by completely different ocean-continent patterns. The first period, 120.4 million years ago, was characterized by high CO_2 concentrations and a continent lying in meridional direction. During the second period, 200 million years ago, a super continent was located in the Northern polar region extending to the South but not reaching the South Pole.

A numerical climate model of intermediate complexity was used in the work. The study is based on the three-dimensional hydrodynamic global climate coupled model, including ocean model with real depths and continents configuration, sea ice evolution model and energy and moisture balance atmosphere model [2, 3].

The ocean model is based on the thermocline (or planetary geostrophic) equations, with the addition of a linear drag term in the horizontal momentum equations. In the resulting frictional geostrophic system, density depends nonlinearly on the local values of temperature and salinity, which obey separate advection-diffusion equations and are also subject to convective adjustment. The model vertical levels are uniformly spaced in the logarithmic coordinate so that the upper layers are thinner, while the horizontal grid is uniform in longitude and in sine of latitude (giving boxes of equal area in physical space). There are 8 density vertical levels on a logarithmically stretched grid with vertical spacing increasing with depth from 140 m to 1120 m. The maximum depth is set to 5 km.

The global climate model is supplemented by a horizontal wind calculation procedure. It takes into account geostrophic, thermal and surface friction wind components. This allows us to qualitatively correctly describe the wind speed field depending on the state of the climate system.

The main parameters of the climate system were determined for the examined two periods. It was established that the climate system reached its steady state in 1500-2000 years. Global and spatial main climatic characteristics for the atmosphere, ocean, and sea ice were obtained. The calculated average global temperature of the atmosphere is within the limits reconstructed from observation data.

The ocean circulation features were studied for the relevant periods. Very strong circulation differences were found for two experiments. This is connected with highly different continents configurations and ocean depths distribution. A strong positive horizontal circulation was detected in the Southern hemisphere and an extended negative circulation was found in the western part of the ocean for the 120.4 million year period. Circulation in the northern part was rather weak. A suppressed circulation was observed in the northern region of the World Ocean accompanied by rather complex circulation patterns in the southern region for the 200 million year period.

This work was supported by the Russian Foundation for Basic Research (grants №16-01-00466, №17-01-00693).

References

1. *Sorokhtin O.G., Ushakov S.A.* Development of the Earth. M: Izd-vo MGU, 2002. 506 p. (in Russian).

2. *Marsh R., Edwards N.R., Shepherd J.G.*. “Development of a fast climate model (C-GOLDSTEIN) for Earth System Science.” SOC, 2002, No.83. 54 p.

3. *Parkhomenko V.P.* “Climate model with consideration World ocean deep circulation,” Vestnik MGTU im. Baumana. Issue Mathematical Modelling, p. 186-200 (2011) (in Russian).

The effect of the Wadden Sea for very high resolution atmospheric regional climate models

Benjamin Schaaf[1], and Frauke Feser[1]
[1] Helmholtz-Zentrum Geesthacht, Centre for Materials and Coastal Research, 21502 Geesthacht, Germany
Corresponding author: Benjamin Schaaf (benjamin.schaaf@hzg.de)

1. INTRODUCTION

Non-hydrostatic climate models such as the COSMO model, which is a limited-area atmospheric prediction model of the German weather service (DWD), are used for simulations with high resolutions (<10 km). There are numerous studies, which show added value (especially for precipitation) for these high-resolution convection-permitting simulations (Prein et al. 2013). But such simulations pose new challenges since they have to take into account mesoscale features and processes in contrast to lower resolution simulations. The Wadden Sea is an intertidal zone in the southeastern part of the North Sea which falls dry and is flooded twice daily, respectively. This study deals with the question if it is necessary to consider the tidal cycle of the Wadden Sea in order to achieve realistic weather states at this high resolution.

2. MODEL SET-UP

For this reason two test simulations with the model COSMO-CLM (CCLM), which is the climate version of the COSMO model, was used (Rockel et al. 2008). The tide cycle and the related change of sea-/land area are not implemented in CCLM. Two simulations were computed with a horizontal grid distance of 1 km, 86 x 82 grid points, and forced by the CoastDat II data set (Geyer 2014) with double nesting. Simulated is the year 1962 which is the year of the big storm surge in Hamburg. One simulation was done in the state “low tide” and one in the state “high tide” which were created by using new land-sea masks. The domain includes the Wadden Sea around the North Frisian Islands of Northern Germany (Figure 1).

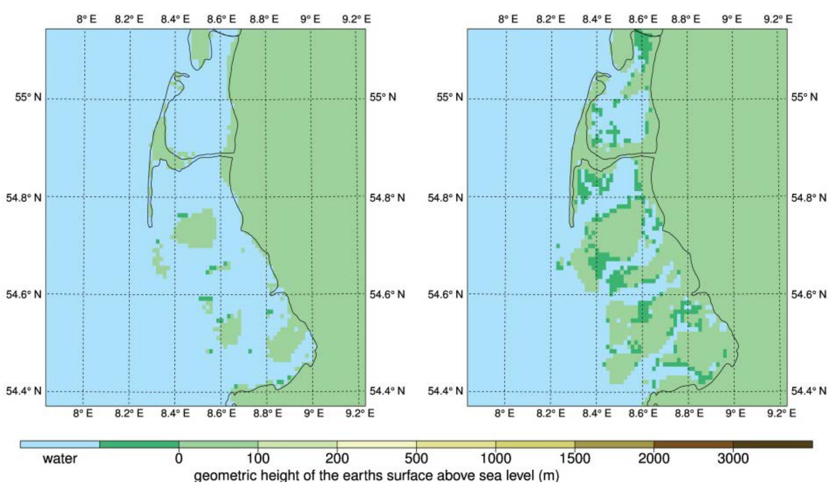

Figure 1: Model domain of the simulations and according topography of the a) “high tide” state and b) “low tide” state.

3. RESULTS

10 m wind speed and 2 m temperature were analyzed. In the low-tide state the mean autumn and winter temperatures are decreased by more than 3 K in the Wadden area. In the winter time the North Sea is warmer than the air temperature and heats the near surface air. This heating does not apply if the sea area falls dry in the low tide state, which results in lower 2 m temperatures (Figure 2). This effect is most pronounced in the Wadden area, but also in the close surroundings a temperature decrease (especially in winter time) is visible, which also extends to the lee side a few kilometers further inland.

On the other hand, the roughness length increases for low tide. Therefore the 10 m wind speed is reduced in this area (up to 1.7 m/s for seasonal mean), especially in seasons with high wind speeds (winter and autumn). In contrast to the 2 m temperature the effect is limited to the areas where the surface type changes from water to land (Figure 3).
Precipitation does not show any significant differences between low and high tide. In this study only the two extreme conditions low and high tide are examined and realistic conditions of continuous change from low to high tide for six hours and back.
Nevertheless, 20% of the grid points fall dry and become flooded in this model domain and should thus be taken into account for grid distances of 1 km and less, although the effect shown in this study is certainly overestimated. The temperature difference is quite large, because the sea level temperature (SST) is taken from NCEP I reanalysis with a resolution of 1.875° (about 200 km). This means, that the whole model domain comprises only parts of a single NCEP grid point. Therefore not only the changes between land and sea should be considered, but also the resolution of the SST should be improved when simulating the Wadden Sea area with this high resolution.

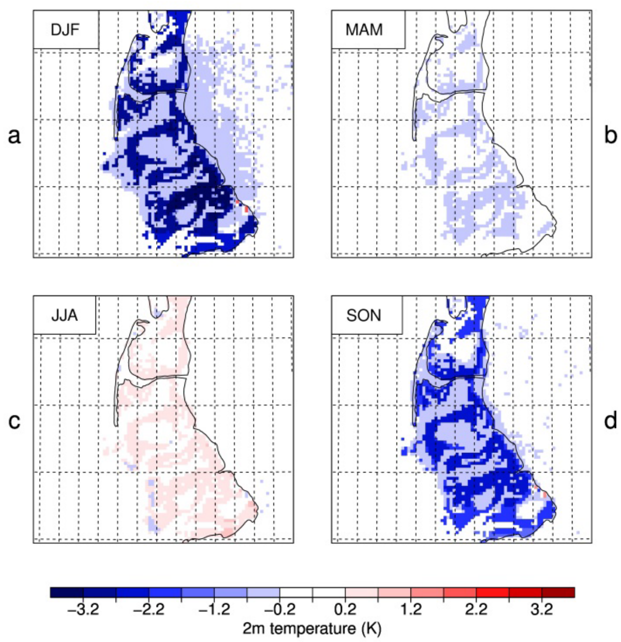

Figure 2: Difference of the seasonal mean 2 m temperature between low and high tide state for a) winter, b) spring, c) summer, and d) autumn.

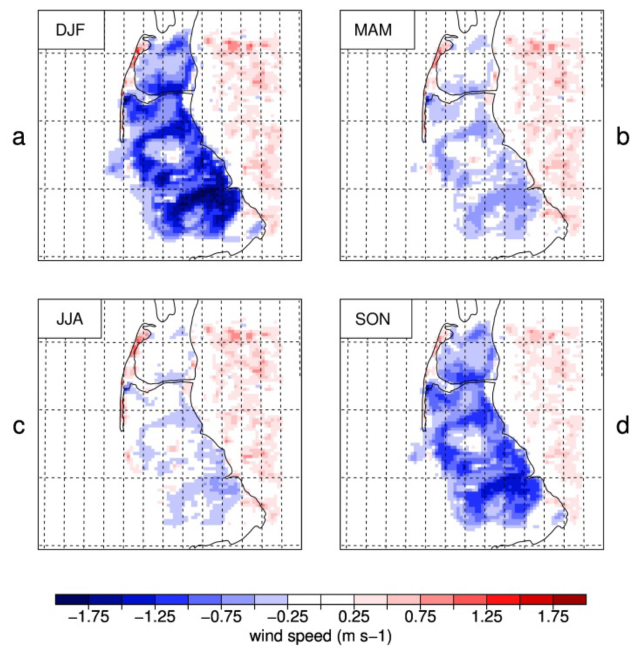

Figure 3: Difference of the seasonal mean 10 m wind speed between low and high tide state for a) winter, b) spring, c) summer, and d) autumn.

REFERENCES

Geyer, B., 2014: High-resolution atmospheric reconstruction for Europe 1948–2012: coastDat2. *Earth Syst Sci Data*, **6**, 147–164, doi:10.5194/essd-6-147-2014.

Prein, A. F., A. Gobiet, M. Suklitsch, H. Truhetz, N. K. Awan, K. Keuler, and G. Georgievski, 2013: Added value of convection permitting seasonal simulations. *Clim. Dyn.*, **41**, 26555–2677, doi:10.1007/s00382-013-1744-6.

Rockel, B., A. Will, and A. Hense, 2008: The Regional Climate Model COSMO-CLM (CCLM). *Meteorol. Z.*, **17**, 347–348.